Journal of Materials Chemistry A

ROYAL SOCIETY OF CHEMISTRY

PAPER

View Article Online
View Journal

Cite this: DOI: 10.1039/d5ta08741d

Unlocking high-performance zinc batteries *via* haloacetamide-regulated nucleation and interface chemistry

Seul Gi Lee,†[a] Syryll Olidan,†[a] Laudimer Tye Tan,[a] Kuk Young Cho,*[b] Jihoon Kim*[a] and Sukeun Yoon*[a]

Lithium-ion batteries dominate the secondary battery market but are increasingly challenged by concerns over safety, sustainability, and critical material dependency. Aqueous zinc metal batteries (AZMBs) offer a compelling alternative for safe, low-cost, and environmentally friendly energy storage. However, their practical deployment is hindered by dendrite formation, hydrogen evolution, and interfacial instability. Here, we introduce haloacetamides as a new class of electrolyte additives that regulate zinc interfacial chemistry at the molecular level. Specifically, iodoacetamide modulates Zn^{2+} solvation and surface reactivity *via* dual coordination with water molecules and Zn^{2+} ions, enabling precise control over nucleation and deposition pathways. This leads to compact, dendrite-free Zn morphology while significantly suppressing hydrogen evolution and corrosion. Notably, iodoacetamide lowers the overpotential from 11 mV to 7 mV, indicating improved reversibility of Zn plating/stripping. As a result, symmetric Zn||Zn cells demonstrate outstanding cycling stability exceeding 2000 h, and full cells maintain over 82% capacity retention for more than 1500 cycles. The additive also enhances high-rate capability by facilitating Zn^{2+} transport and interfacial uniformity. This study presents a previously unexplored strategy for tuning Zn interfacial behavior through halogenated molecular design, representing a promising route for aqueous battery additive development. Our findings highlight haloacetamides as a powerful platform for interphase engineering toward durable, high performance AZMBs.

Received 28th October 2025
Accepted 14th January 2026

DOI: 10.1039/d5ta08741d

rsc.li/materials-a

1 Introduction

Lithium-ion batteries (LIBs) dominate the energy-storage market; however, they face several limitations, including a reliance on scarce and geopolitically sensitive materials, safety risks associated with thermal runaway, and environmental concerns. These challenges have driven the development of alternative technologies, such as all-solid-state batteries (ASSBs); however, ASSBs encounter similar obstacles, including material scarcity, manufacturing complexities, and interface stability issues, which hinder their commercialization.[1–3] Aqueous metal-ion batteries have the benefit of a high theoretical volumetric energy density because they can utilize the reaction of polyvalent metal ions such as Mg^{2+}, Ca^{2+}, Zn^{2+}, and Al^{3+}. In addition, the ion-supplying metals used in these batteries have greater natural abundance than lithium and lower raw material costs, making these systems both economical and safe.

Specifically, rechargeable aqueous Zn metal batteries (AZMBs) are relatively safer, offer a high capacity (820 mAh g^{-1} or 5850 mAh cm^{-3}), utilize an abundant resource (70 ppm in the Earth's crust), and exhibit favorable economic and eco-friendly characteristics. As a result, AZMBs are gaining more attention and undergoing rapid development compared to other multivalent metal-ion batteries.[4–6] Nevertheless, AZMBs fundamentally suffer from a relatively low thermodynamic Zn^{2+}/Zn redox potential (−0.76 V *vs.* SHE) compared to the onset potential of the H_2O/H_2 redox reaction. This leads to undesirable side reactions, including the hydrogen evolution reaction (HER), Zn metal passivation and corrosion, and Zn dendrite formation. These reactions are difficult to control under the harsh operating conditions of charging and discharging, which significantly reduce the reversible performance of the battery.[7–9] Therefore, the transformation of traditional Zn-based primary batteries into reliable rechargeable batteries remains a persistent scientific challenge. Recent efforts to address these issues include three-dimensional Zn structural designs, membrane technologies, artificial protective layers, and electrolyte engineering. Notably, these issues occur predominantly at the

[a]Division of Advanced Materials Engineering, Kongju National University, Chungnam 31080, Republic of Korea. E-mail: jihoon.kim@ kongju.ac.kr; skyoon@kongju.ac.kr
[b]Department of Materials Science and Chemical Engineering, Hanyang University ERICA, Gyeonggi 15588, Republic of Korea. E-mail: kycho@hanyang.ac.kr
† These authors contributed equally.

interface between the Zn metal anode and the electrolyte, making electrolyte optimization one of the simplest and most effective strategies.[10–13]

Aqueous electrolytes generally use $ZnSO_4$ and $Zn(CF_3SO_3)_2$ salts in neutral and mildly acidic environments, respectively. These salts meet the basic requirements of excellent solubility, high ionic conductivity, interfacial wettability, and compatibility with electrode materials. However, they are susceptible to water decomposition at relatively low voltages, which hinders their combination with high-voltage cathode materials, resulting in significantly lower energy densities. In addition, neutral or slightly acidic environments cause problems, such as the corrosion and degradation of Zn metal anodes and collectors, resulting in shorter battery lifespans.[14–16] To address this issue, high concentrations of Zn salt have been proposed to improve the electrochemical performance of AZMBs. Increased salt concentrations can lower the activity of water molecules, thereby inhibiting degradation reactions and improving electrolyte stability during cycling, thus enhancing the coulombic efficiency (CE) and operating lifetime. Therefore, increasing the electrolyte salt concentration is also considered a way to overcome the narrow operational voltage window (below 2 V) of conventional electrolytes, ultimately improving energy density.[17,18] Another effective solution for improving the performance of AZMBs is the addition of electrolyte additives. The four main types of additives include organic molecules (*e.g.*, saccharin, glucose, arginine, sodium dodecyl sulfate, and urea), organic solvents (*e.g.*, ethylene glycol, acetonitrile, dimethyl carbonate, and benzylidene acetone), ionic liquids (*e.g.*, [EMIM][DCA], [EMIM][OTf], [EMIM][TFSI], and $EMIMBF_4$), and metal ions (*e.g.*, Na, Ag, Sn, and Sb).[19–25] These additives are added in small quantities to the electrolyte to suppress anode dissolution, promote consistent Zn plating/stripping to prevent dendrite formation, and establish a stable solid electrolyte interphase (SEI). Additionally, certain additives have been used to extend the operational voltage range by changing the solvation structure of the electrolyte, thereby boosting the energy density.

In particular, anionic chemistry is of growing interest because modifying the electrolyte with specific anions can impart unique functionalities to battery systems while preserving the original electrode structure. Additionally, this approach can contribute to ionic (de)solvation effects, which help enhance the dynamics of solid–liquid interfacial reactions. For instance, SO_4^{2-} anions in Zn–TiN capacitors participate in a two-step adsorption and insertion process, enhancing self-discharge prevention and stable capacitance performance.[26] Cluster models, such as $[Zn(TfO)_4]^{2-}$ and $CF_3SO_3^-$, enable stable reversibility and fast deposition/dissolution dynamics owing to their low solvation energy and high solubility.[27,28] Cl^- ions bind tightly to dimethyl sulfoxide (DMSO) molecules, forming $Zn_{12}(SO_4)_3Cl_3(OH)_{15}\cdot 5H_2O$ and ZnS-enriched solid electrolyte interphases (SEIs), thereby maintaining cycling stability.[29] Finally, the oxidation of iodine can remove Zn dendrites from the separator through redox reactions, preventing micro-short circuits.[30]

Herein, we investigate the effect of haloacetamides as electrolyte additives on the electrochemical properties of AZMBs, aiming to modify the Zn anode–electrolyte interface, stabilize Zn ion electrodeposition, and suppress unwanted byproducts. Experiments and calculations indicate that certain halide anions form distinct surface solvation structures and accumulate at high concentrations at the interface owing to their strong polarizability.[31] These ions tend toward the electrode interface, adsorb, and create an anion-rich Zn surface.[32] Halide ions occupy the active sites involved in water-induced side reactions, suppressing both the HER and Zn corrosion. Distribution of relaxation time (DRT) analysis revealed a decrease in the resistance component (R_{ad}) associated with Zn^{2+} ion desolvation and adsorption, suggesting that the additives facilitate Zn^{2+} desolvation, promoting smooth Zn deposition and suppressing non-uniform Zn dendrite growth.[33] Furthermore, these additives form a stable SEI during battery cycling, thereby preventing side reactions and uncontrolled Zn dendritic growth.[34] Consequently, Zn||Zn symmetric cells exhibited significantly improved electrochemical performance, with an overpotential as low as 7 mV and a stable cycling performance for 2000 h at 1 mA cm^{-2}. In this study, Zn||activated carbon batteries containing halide ions showed improved self-discharge resistance and cycling stability, highlighting a promising new strategy for stabilizing the metal–electrolyte interface in AZMBs.

2 Experimental

2.1 Electrolyte preparation

The base electrolyte used was an aqueous solution containing 1 M zinc sulfate ($ZnSO_4\cdot 7H_2O$) with a pH value of 4.51. Analytical grade haloacetamides (HAAs) (Alfa Aesar), including trifluoroacetamide (TFAA), chloroacetamide (CAA), bromoacetamide (BAA), and iodoacetamide (IAA), were dissolved in the base electrolyte at various concentrations. Simple halide salts (Sigma-Aldrich), sodium bromide (NaBr), and sodium iodide (NaI) were added to the base electrolyte at comparable concentrations with their HAA counterpart.

2.2 Material characterization

The crystalline phases of the Zn deposits were determined by X-ray diffraction (XRD; Rigaku SmartLab, Cu Kα radiation). The chemical composition of the surface was characterized by X-ray photoelectron spectroscopy (XPS; Thermo Fisher Scientific, Al Kα radiation). The morphology, microstructure, and composition of the samples were analyzed using field-emission scanning electron microscopy (FE-SEM; Carl Zeiss, SIGMA 500). Zeta potentials were measured using a Malvern Zetasizer Nano ZSP. Contact angle analysis was performed five times on average by dropping 15 μL of electrolyte into different positions and measuring the angle using an SEO Phoenix 300. The pH of the electrolytes was measured using an OHAUS Starter 2100 pH meter. UV-vis spectroscopy was performed using an OPTIZEN POP. The Zn ion transference number ($t_{Zn^{2+}}$) was calculated from the chronoamperometry and EIS results using the Bruce–Vincent–Evans equation. Real-time Zn plating/stripping

experiments were conducted using a lab-made *in situ* symmetric cell, and snapshots were captured using a digital optical microscope (Siwon Optical, Dimis-M5).

2.3 Electrochemical measurements

Zn||Cu half-cells were assembled to analyze the Zn plating/stripping behavior of different electrolyte designs when cycled at 1 mA cm^{-2} (0.5 mAh cm^{-2}) using a Maccor 4000 battery tester. Meanwhile, the charge–discharge characteristics of Zn||Zn symmetric cells were evaluated *via* chronopotentiometry at a constant current density of 1 mA cm^{-2} on battery cyclers (Maccor 4000 and LANHE G340A). The cathode was fabricated by mixing 80 wt% activated carbon (AC, CEP21K), 10 wt% carbon black (Super P), and 10 wt% PVDF in NMP. The resulting mixture was then coated onto a 10 μm titanium foil (Goodfellow), vacuum dried at 60 °C for 6 h, and then pressed. A coin cell (CR2032) was assembled using a Zn metal anode, a Whatman glass microfiber filter separator, and an electrolyte with or without additives. Galvanostatic charge–discharge tests were performed at 2 A g^{-1} (based on AC) within a voltage range of 1.8–0.2 V *vs.* Zn^{+}/Zn after 12 h rest time after cell assembly. Cyclic voltammetry (CV) tests were performed using a LANHE G340A battery tester at various scan rates. Electrochemical impedance spectroscopy (EIS) was performed using a PARSTAT 4000 instrument over a frequency range of 100 kHz to 0.1 Hz with a 10 mV amplitude signal. The results were fitted using ZSimpWin software, and the raw EIS data were further analyzed using the DearEIS GUI program to extract the DRT graphs.[35] Linear sweep voltammetry (LSV) and Tafel analysis were performed using ZIVE SP2 equipment in an electrolyte with Zn metal (or glassy carbon), graphite, and a saturated calomel electrode as the working, counter, and reference electrodes, respectively, at a scan rate of 5 mV s^{-1}.

2.4 Computational details

The molecular orbital energy calculations for HAAs and water were performed using the Gaussian 16 W program package using the B3LYP functional with the 6-31G basis set and the DGDZVP method. Adsorption energy calculations were carried out using the PWscf code in the Quantum ESPRESSO 6.4 package, with the spin polarization modeled using the projector augmented wave (PAW) method and a generalized gradient approximation based on the Perdew–Burke–Ernzerhof (GGA-PBE) exchange–correlation functional.[36] The wavefunction cutoff energy was set to 30 Ry, and Gaussian broadening was set to 0.002 Ry. All structures were relaxed until the force and energy on each atom reached 0.00038 Ry $bohr^{-1}$ and 10^{-7} Ry, respectively. Brillouin zone integration was performed using the $4 \times 4 \times 1$ Monkhorst–Pack *k*-point grid sampling. A Zn (002) supercell with six atomic layers was constructed, with a 15 Å vacuum layer along the *c*-axis (perpendicular to the surface). Finally, the adsorption energy (E_{ads}) was calculated using the equation: $E_{ads} = E_{tot} - (E_{Zn} + E_{add})$, where E_{tot} is the total energy after adsorption of HAAs or water on the zinc slab, E_{Zn} is the energy of the Zn (002) surface, and E_{add} is the energy of HAAs or water.

The current density distribution was simulated using COMSOL Multiphysics 6.2, employing the secondary current distribution module. The Butler–Volmer equation and Nernst–Einstein relation were applied to simulate electrode kinetics and ionic migration in the presence of an electric field.[37,38] The electrodes were set at a thickness of 1.5 μm, and the electrolyte height was set to 5 μm. Surface irregularities on the electrode were modeled as ellipses with a constant height of 0.5 μm. For electrolytes with additives, rectangular bars were placed on top of the electrode surface to represent the adsorbed HAA.[39] Only IAA was used to represent the additive-containing system, as the differences among other HAAs were negligible and the adsorption mechanism remained consistent. Conductivities for 1 M $ZnSO_4$ and 1 M $ZnSO_4$ + 0.5 M IAA were 46.1 and 40.8 mS cm^{-1}, respectively. The initial potential was set to 0 V for the electrodes, with all other surfaces treated as insulators. The secondary current distribution module was coupled with the transport of the dilute species module to solve the Nernst–Planck equation. The initial ion concentration was set to 2000 mol m^{-3}. Note that the simulations were performed to primarily highlight the effect of additive adsorption on the electrode surface under extremely ideal conditions, except where otherwise mentioned.

3 Results and discussion

Density functional theory (DFT) calculations were conducted to evaluate the potential of haloacetamides (HAAs), including trifluoroacetamide (TFAA), chloroacetamide (CAA), bromoacetamide (BAA), and iodoacetamide (IAA), as electrolyte additives for stabilizing Zn metal anodes in aqueous batteries. The molecular orbital levels of all HAAs lie between the lowest unoccupied molecular orbital (LUMO) and the highest occupied molecular orbital (HOMO) of H_2O, except for the HOMO of TFAA (Fig. 1a). This suggests that HAAs can effectively inhibit water decomposition and promote the adsorption of ionized molecules on the Zn surface.[40] Although the exact mechanism of halide ion interactions with Zn metal is not yet fully elucidated, valuable insight can be obtained from the well-established reactivity of zero-valent metals (ZVMs), such as Fe, Sn, Al, and Zn, toward halogen-containing species.[41,42] In ZVM systems, halide ions would facilitate the deposition of metal cations in solution by forming intermediates between the metal surface and the metal ions. When chlorinated organics come into contact with ZVMs, thermodynamically favorable reductive dehalogenation occurs, releasing halide ions into the solution and either dissolving or precipitating oxidized metal ions. In this reaction, the ZVM provides electrons, effectively mimicking a corrosion-like process. Based on this principle, the reaction mechanisms of HAA decomposition, halogenation, and hydration in the present system could be described as follows:[43–45]

$$XCH_2CONH_2 + H_2O + Zn^0 \rightarrow CH_3CONH_2 + Zn^{2+} + OH^- + X^- \quad (1)$$

$$2\,Zn^0 + 2\,H_2O + O_2 \rightarrow 2\,Zn^{2+} + 4\,OH^- \quad (2)$$

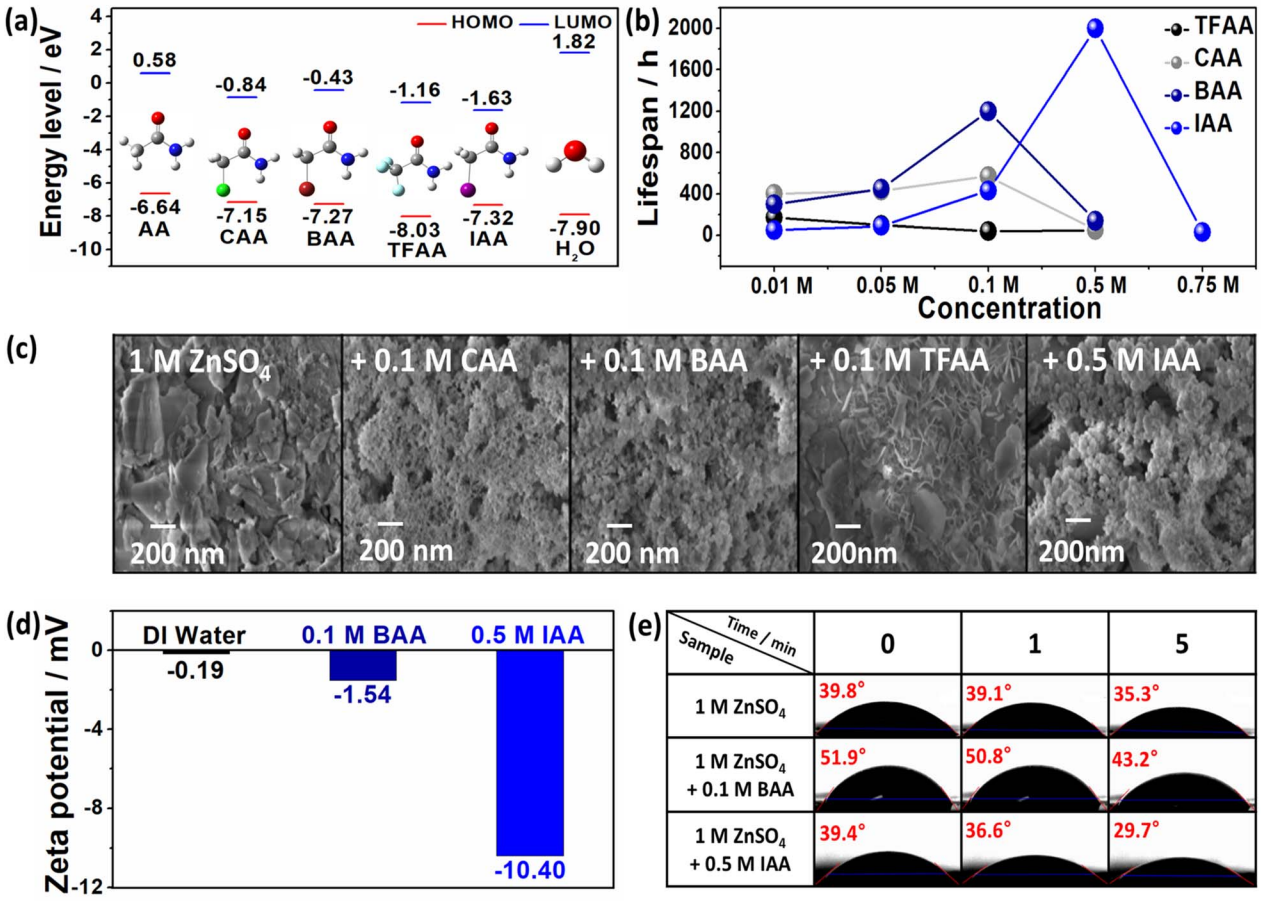

Fig. 1 (a) Calculated HOMO and LUMO energy levels of acetamide, haloacetamides, and water. (b) Lifespan of Zn||Zn symmetric cells with different concentrations of haloacetamide additives in 1 M $ZnSO_4$ at 1 mA cm^{-2} (1 mAh cm^{-2}). (c) SEM images of Zn metal electrodes after 100 cycles in 1 M $ZnSO_4$ electrolyte with and without haloacetamides. (d) Zeta potential of Zn powder and (e) contact angle of 1 M $ZnSO_4$-based electrolytes on Zn metal surfaces, measured with and without bromoacetamide or iodoacetamide.

$$XCH_2CONH_2 + H_2O \xrightarrow{OH^-} XCH_2COOH + NH_3 \quad (3)$$

$$XCH_2COOH + H_2O + Zn^0 \rightarrow CH_3COOH + Zn^{2+} + OH^- + X^- \quad (4)$$

where X denotes a halide species. In this system, Zn would act as the ZVM to ionize the haloacetamide *via* reductive dehalogenation (eqn (1)), which would result in the migration of Zn and the formation of acetamide. The OH^- released from the redox reaction (eqn (2)) would then facilitate hydrolysis reactions, yielding haloacetic acid and acetic acid as byproducts (eqn (3) and (4)).

To understand the effect of halide ions on the Zn metal during the electrochemical reaction, the optimal concentration of each additive was first determined by cycling a Zn||Zn symmetric cell at a current density of 1 mA cm^{-2} (1 mAh cm^{-2}) (Fig. S1–S5). Based on the results, the following concentrations were selected for further analysis: 0.01 M TFAA, 0.1 M CAA, 0.1 M BAA, and 0.5 M IAA. These were identified as optimal based on their superior cycling performance. Fig. 1b summarizes the cycling lifespans of Zn||Zn symmetric cells incorporating the optimal additive concentrations. Among the four, TFAA (0.01 M) exhibited the shortest lifespan, failing after 180 h. In contrast, cells with CAA (0.1 M), BAA (0.1 M), and IAA (0.5 M) demonstrated significantly enhanced stability, sustaining cycling for 580, 1050, and 2000 h, respectively. To further investigate the morphological changes, the Zn metal electrodes after 100 cycles were examined by SEM (Fig. 1c). The Zn surfaces cycled in the electrolytes containing CAA, BAA, or IAA were uniformly covered with small, granular particles, suggesting compact Zn deposition. In contrast, the surfaces of electrodes cycled in the base electrolyte or with TFAA exhibited prominent hexagonal platelets, which is a characteristic of dendritic growth and byproduct formation. These results confirm that CAA, BAA, and IAA effectively inhibit Zn dendrite formation compared to TFAA, which is consistent with the symmetric cell cycling performance. Therefore, all subsequent electrochemical measurements were conducted using BAA- and IAA-containing electrolytes, as they showed relatively superior performance among the HAA derivatives. To evaluate the role of acetamide in this performance improvement, control electrolytes with simple halide salts were prepared at comparable concentrations with BAA and IAA. As shown in Fig. S6, the Zn

symmetric cell containing 0.1 M NaBr in 1 M $ZnSO_4$ electrolyte failed after 40 h of cycling, worse than the performance of the base electrolyte. In contrast, when 0.5 M NaI was added, the cycle life was extended beyond that of the base electrolyte and NaBr. However, a gradual increase in voltage hysteresis after 180 h can be observed which is indicative of growing cell impedance. From these comparisons, it can be deduced that iodine is more beneficial than bromine for improving the cycling performance of Zn symmetric cells regardless of the chemical species that they are with (Na or acetamide). Furthermore, these findings demonstrate that the performance enhancement is driven by the intrinsic reactivity of haloacetamides, not simply by the presence of halide anions. In the CV curves of the Zn-based symmetric cells with BAA and IAA (Fig. S7), no specific oxidation/reduction peaks are present, indicating capacitive adsorption. This suggests that HAAs can influence Zn plating/stripping reactions by controlling the interfacial charge at the Zn anode.

To verify the electrostatic adsorption properties of I^- and Br^- on Zn metal, zeta potential was measured. As shown in Fig. 1d, the potential values of BAA and IAA decrease from −0.19 mV, based on pure water, to −1.54 and −10.40 mV, respectively. These relatively more negative values confirm the electrostatic adsorption of halide anions on the zinc metal surface. These halide ions can easily form solvated structures due to their strong nucleophilicity, which may lead to desolvation of Zn and uniform Zn deposition. Furthermore, the wettability of the electrolytes was measured to confirm the affinity of HAAs to Zn metal. As shown in Fig. 1e, the initial contact angles of the electrolytes containing BAA and IAA with respect to the Zn surface were 51.9° and 39.4°, respectively, and decreased to 43.2° and 29.7° after 5 min. The reduced contact angle compared to the base electrolyte suggests that a favorable halide anion-rich Zn surface exists. The improved wettability and interfacial adsorption behavior of BAA and IAA suggest that these additives can facilitate uniform nucleation and deposition of Zn^{2+} by lowering the interfacial free energy between the Zn metal and the electrolyte.

A schematic diagram of the discussed mechanism is presented in Fig. 2a. In the absence of additives, Zn^{2+} ions deposit onto the initial protuberances on the Zn surface, growing vertically and forming dendrites. Water molecules can also interact freely with Zn, which aggravates side reactions, resulting in the formation of byproducts, hydrogen gas evolution, and corrosion. By contrast, incorporating HAAs into the electrolyte can modulate the Zn surface through redox reactions with Zn^0. Emphasizing on the plausible mechanism of haloacetamides (eqn (1)–(4)), the liberated halide ions are adsorbed onto the Zn surface, preventing direct contact between Zn and water and thereby suppressing undesirable side reactions. In addition, HAAs could scavenge OH^- ions and convert them into haloacetic and acetic acids, preventing them from reacting with Zn to form byproducts. As a result, uniform Zn deposition is achieved due to the homogenized current density distribution at the Zn surface induced by halide ion adsorption. To validate this behavior, COMSOL simulations were conducted to understand the dynamic Zn^{2+} deposition process. As shown in Fig. 2b, the electric field is concentrated at the tips of the initial protuberances, which act as hotspots for Zn^{2+} ions and promote vertical growth until the deposits puncture the separator and cause short circuits. In contrast, the presence of additives alters the Zn^{2+} deposition behavior by distributing the current density more evenly across the surface, thereby alleviating the tip effect observed in the base electrolyte (Fig. 2c). As a result, uniform Zn plating is achieved.

LSV and potentiodynamic polarization measurements were carried out to examine the effects of BAA and IAA on side reactions, particularly the hydrogen evolution reaction (HER)

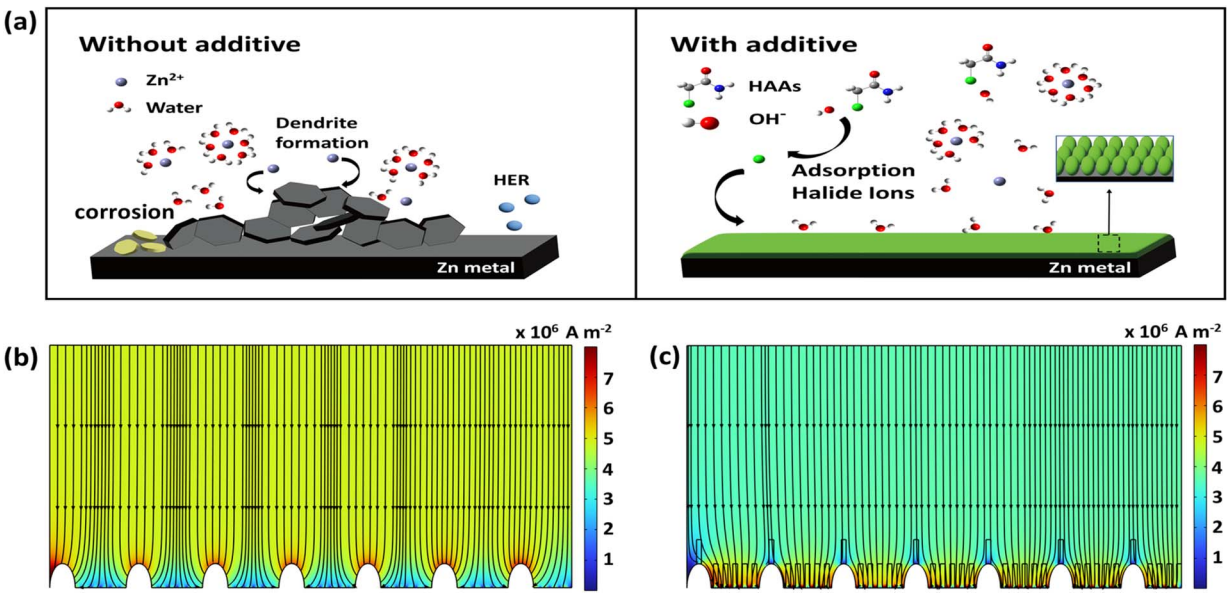

Fig. 2 (a) Schematic illustration showing the protective mechanism of haloacetamide additives. (b and c) COMSOL simulations of Zn^{2+} flux distribution in (b) 1 M $ZnSO_4$ electrolyte and (c) 1 M $ZnSO_4$ electrolyte containing haloacetamides.

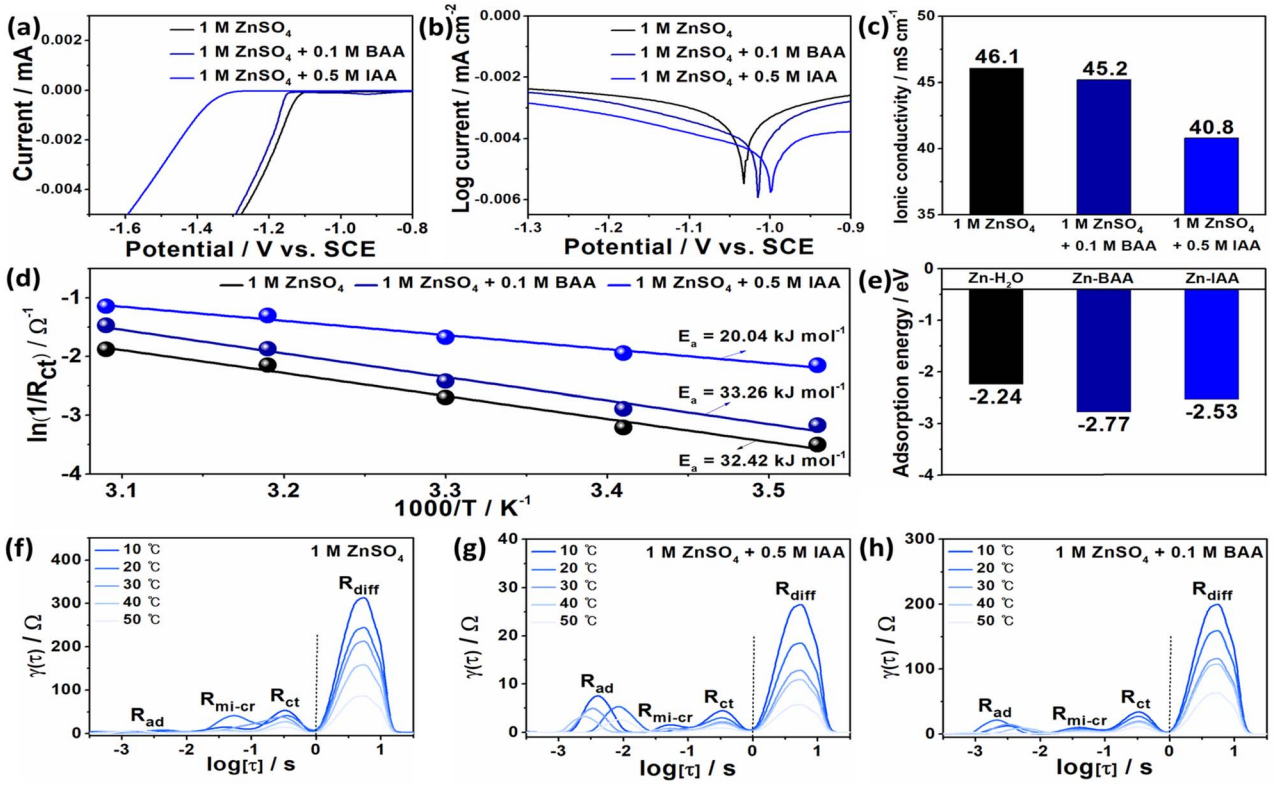

Fig. 3 (a) LSV, (b) potentiodynamic polarization curves, and (c) ionic conductivity of 1 M $ZnSO_4$ electrolytes with and without bromoacetamide or iodoacetamide. (d) Arrhenius plots derived from R_{ct} values at various temperatures, showing the desolvation activation energies. (e) Calculated adsorption energies of iodoacetamide, bromoacetamide, and water in 1 M $ZnSO_4$ electrolytes. (f–h) Temperature-dependent EIS spectra and corresponding DRT analysis of 1 M $ZnSO_4$ electrolytes: (f) without additives, (g) with iodoacetamide, and (h) with bromoacetamide.

and Zn corrosion. As shown in Fig. 3a, the onset potential for the HER in the presence of BAA and IAA shifts negatively to approximately −1.35 V and −1.15 V, respectively, indicating increased HER overpotential. Potentiodynamic polarization curves (Fig. 3b) show that the corrosion potential shifts positively to −1.00 V and −1.02 V, while the exchange current density decreases to −0.0045 and −0.0041 mA cm^{-2}, respectively. These results suggest that both the HER and corrosion of Zn at the interface are effectively suppressed by the additives. Fig. 3c shows that the addition of BAA and IAA to the electrolyte slightly decreases the ionic conductivity to 40.8 and 45.2 mS cm^{-1}, respectively. Meanwhile, the calculation of Zn ion transference number ($t_{Zn^{2+}}$) from the chronoamperometry curves and Nyquist plots revealed that the values increase to 0.594 and 0.609 for BAA and IAA, respectively, from 0.362 exhibited by the base electrolyte (Fig. S8 and S9). This implies that while the total ion mobility is slightly hindered due to higher solute concentration, a greater proportion of Zn^{2+} ions contributes to charge transport.[46]

To further quantify Zn^{2+} transport, the activation energy (E_a) was calculated using the Arrhenius equation, based on resistance measurements at different temperatures (Fig. S10–12). The linear fits in Fig. 3d indicate that the introduction of IAA reduces E_a to 20.04 kJ mol^{-1}, whereas BAA increases E_a to 33.26 kJ mol^{-1}, compared with that of the base electrolyte (32.42 kJ mol^{-1}). This trend is consistent with the overpotentials observed during cycling of the Zn-based symmetric cell: base electrolyte (11 mV), BAA (40 mV), and IAA (7 mV) (Fig. S13). The activation energy refers to the energy required to initiate Zn^{2+} plating/stripping, and the nucleation overpotential refers to the potential required to start deposition. Since the addition of IAA results in the lowest E_a, it requires the least driving force for initial Zn deposition, unlike the addition of BAA or the base electrolyte, which requires higher potentials. These characteristics may relate to adsorption energy; however, they are not exclusively connected. The calculated adsorption energies for BAA (−2.77 eV) and IAA (−2.53 eV) are lower than that of water (−2.24 eV) (Fig. 3e), indicating that halide ions preferentially adsorb onto the Zn surface. This preferential adsorption prevents water molecules from directly interacting with the Zn metal, thereby forming a water-deficient inner Helmholtz plane (IHP).[47] BAA shows the strongest affinity to Zn metal, suggesting it can hinder ion mobility and block some active Zn sites, resulting in a higher overpotential and activation energy. In contrast, IAA achieves a lower activation energy than that achieved by BAA despite its stronger adsorption to zinc. This observation means that a higher or lower activation energy does not dictate whether the battery performance will be better than the other, as proven by BAA and IAA which both performed better than BE regardless of the value of E_a. Similarly, some reported additives increase or decrease E_a; however, the electrochemical performance of an additive-containing system

is always superior to that of the system using the base electrolyte.[48–51] The resistance of the special solvation structure of Zn^{2+} was further investigated using DRT analysis, based on the same temperature-dependent resistance data utilized for the E_a calculations. The DRT results reveal four distinct resistance peaks, corresponding to different physical interfaces in order of increasing relaxation time constant (Fig. 3f–h). The diffusion of Zn^{2+} ions into the Zn-depositing electrode (R_{diff}) can be attributed to the adsorption and desolvation of Zn^{2+} ions (R_{ad}), charge transfer across the Zn–SEI interface (R_{ct}), and migration of $Zn^{2+}/Zn^{+}/Zn$ species and crystal formation on the Zn surface ($R_{mi\text{-}cr}$).[52,53] Electrolytes containing BAA and IAA exhibit lower R_{diff} and R_{ct}, indicating reduced impedance and improved Zn^{2+} migration, enabling smoother charge transfer and increased interfacial stability, thereby suppressing dendrite formation. The influences of BAA and IAA were further confirmed by *in situ* optical microscopy of the Zn electrode (Fig. S14). Even after 30 min of Zn plating at 3 mA cm^{-2}, the HER and dendrite formation were suppressed owing to the competitive reaction between the halide species and Zn ions, leading to the formation of a uniform and dense passivation layer at the electrode–electrolyte interface. These findings are in line with the measured pH values of the electrolyte blends, showing an increase in H^{+} concentration (Fig. S15). A lower pH implies reduced OH^{-} availability, minimizing reactions with zinc species and subsequent formation of byproducts.

By examining the effect of BAA and IAA additives on the Zn plating/stripping reaction, Fig. 4a presents a comparison of the cycling performances of the electrolytes. The IAA additive enabled the Zn electrode to achieve stable cycling for over 2000 h, whereas the BAA additive allowed the Zn electrode to maintain its stability for up to 1050 h before exhibiting voltage fluctuations and short circuits. Additionally, a stable cycle life of up to 250 h was achieved by IAA and BAA at a high current density of 5 mA cm^{-2} (5 mAh cm^{-2}) (Fig. S16), with stable low-voltage hysteresis values of 58 mV and 77 mV, respectively, owing to rapid zinc kinetics (Fig. 4b and c). Similar behavior can be observed over a wide range of current densities (1, 3, 5, and 10 mA cm^{-2}) in the Zn plating/stripping curves shown in Fig. 4d, demonstrating stable multirate performance and reversible cycling as a result of uniform Zn deposition. Additionally, Zn||Cu half cells demonstrate that the additives induce better plating/stripping reversibility as seen from the extended life of BAA and IAA. Although BAA experienced slight instability after 100 h, it recovered and lasted longer than the base electrolyte which failed after 220 cycles. Meanwhile, IAA showed a stable performance all throughout (Fig. S17–19). Further electrochemical performance assessment of the Zn symmetric cell was performed *via* EIS after the 50th cycle at a current density of 1 mA cm^{-2} (Fig. 4e). The surface resistance (R_s) and charge transfer resistance (R_{ct}) values for the symmetric cell using IAA in the high- and low-frequency regions are 0.5 and 1.0 Ω, respectively, and those for BAA are 1.2 and 2.3 Ω, respectively. This indicates that both BAA and IAA contribute to the formation of a stable interfacial layer during the plating/stripping process and enhance the electron transport effect, improving the overall electrochemical performance.

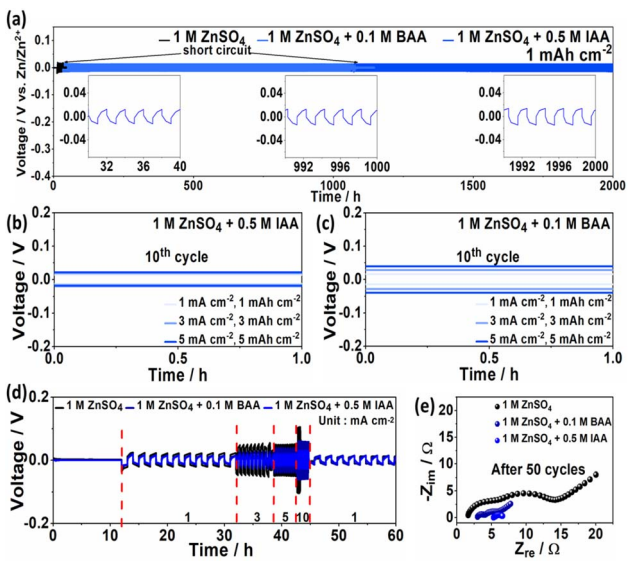

Fig. 4 (a) Galvanostatic cycling performance of Zn||Zn symmetric cells in 1 M $ZnSO_4$ electrolytes with and without bromoacetamide or iodoacetamide at 1 mA cm^{-2} (1 mAh cm^{-2}). (b and c) Voltage profiles of Zn||Zn symmetric cells with (b) iodoacetamide and (c) bromoacetamide at 1, 3, and 5 mA cm^{-2}, recorded after 10 cycles. (d) Multirate cycling performance at a fixed areal capacity of 1 mAh cm^{-2}. (e) EIS spectra of Zn||Zn symmetric cells after 50 cycles in 1 M $ZnSO_4$ electrolytes with and without additives.

To gain insight into the surface composition at the interface underlying the effects of the BAA and IAA additives on dendrite formation and side reactions, XPS analysis was performed on the Zn metal electrode after 10 cycles. The XPS survey spectra in Fig. 5a–c show the presence of peaks related to C 1s, Zn 2p, and S 2p. In the C 1s spectrum (Fig. 5d), a metal carbonate-related peak can be observed at 290 eV, which can be attributed to $ZnCO_3$, in comparison to the $ZnSO_4$ base electrolyte.[54] In the Zn 2p spectrum (Fig. 5e), symmetric doublets corresponding to Zn $2p_{3/2}$ and Zn $2p_{1/2}$ can be identified, with a shoulder peak attributed to ZnO appearing at lower binding energies. Although ZnO was present on the surface of the Zn metal regardless of the additive, its peak was comparatively less intense than that in the base electrolyte, indicating that fewer ZnO species were formed. Additionally, in the S 2p spectrum (Fig. 5f), spin–orbit coupling peaks of sulfate can be observed at 170 eV and 168.85 eV, corresponding to S $2p_{3/2}$ and S $2p_{1/2}$, respectively. Furthermore, the presence of additives significantly reduces the intensity of the S 2p signal, indicating decreased formation of zinc hydroxy sulfate (ZHS) on the Zn plate.[55,56] *Ex situ* XPS analysis revealed that zinc electrodes cycled in electrolytes containing HAAs exhibit notable suppression of sulfate- and hydroxide-related species, indicating a more stable interfacial composition and reduced parasitic reactions. Complementary XRD analysis (Fig. S20) confirmed a distinct phase transformation alongside the presence of ZHS phases. The hydrated $Zn_4SO_4(OH)_6 \cdot 5H_2O$ phase, typically linked to uncontrolled surface hydrolysis and the formation of porous, inactive byproducts, was no longer detected.[57] Instead, the denser $Zn_4SO_4(OH)_6 \cdot 4H_2O$ phase

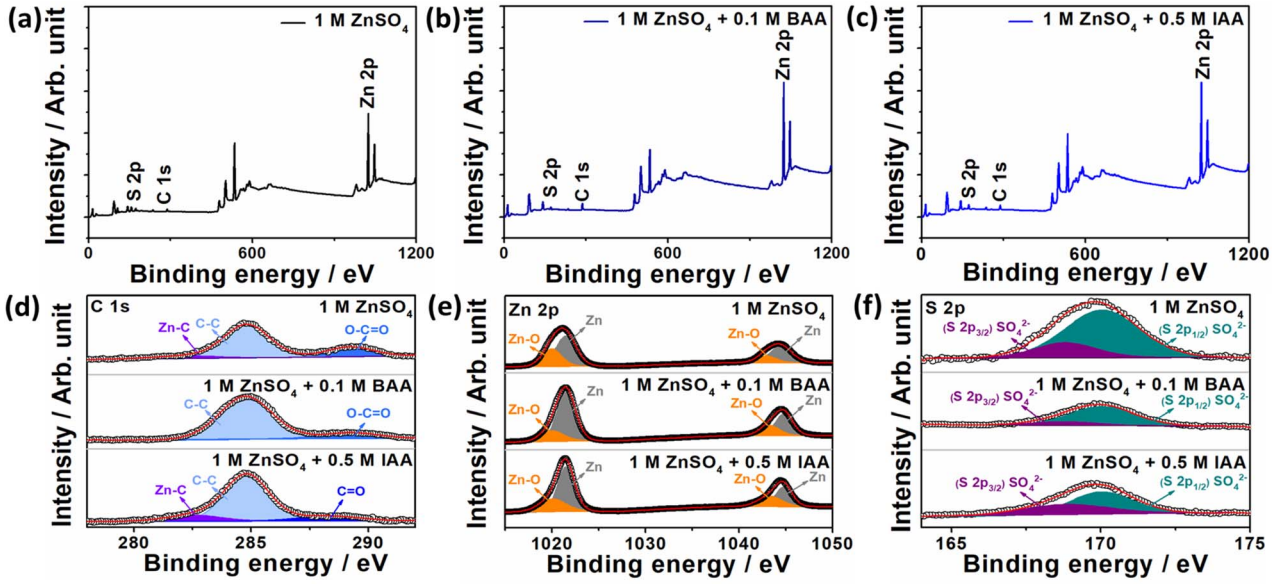

Fig. 5 (a–c) XPS survey spectra of Zn metal electrodes after 10 cycles in (a) 1 M $ZnSO_4$ electrolyte, (b) 1 M $ZnSO_4$ electrolyte with bromoacetamide, and (c) 1 M $ZnSO_4$ electrolyte with iodoacetamide. (d–f) High-resolution (d) C 1s, (e) Zn 2p, and (f) S 2p XPS spectra of Zn metal measured after 10 cycles in 1 M $ZnSO_4$ electrolytes with and without bromoacetamide or iodoacetamide.

emerged as the predominant species. This shift suggests that HAA additives do not eliminate ZHS formation but regulate the crystallization pathway during Zn plating/stripping. This stabilization may be attributed to two synergistic effects of HAA: (i) scavenging of hydroxide ions, which suppresses local alkalinity and prevents overhydrated ZHS precipitation, and (ii) adsorption of halide ions released from HAA decomposition onto the Zn surface, forming a protective interphase that mitigates water-induced side reactions. The selective formation of $Zn_4SO_4(OH)_6\cdot 4H_2O$ serves as compelling evidence that HAAs facilitate a more compact and stable surface layer, consistent with the improved cycling stability and suppressed dendrite formation observed in HAA-containing systems.[58,59] Additionally, the optical and SEM images (Fig. S21) showed that the Zn metal immersed in the electrolytes containing BAA and IAA for five days forms smaller particles and fewer hexagonal plates than those observed in the base electrolyte, indicating enhanced resistance to self-corrosion.

The effectiveness and practicality of BAA and IAA were investigated using a Zn||AC full cell. The CV curves for the BAA and IAA electrolytes (Fig. 6a and b) exhibit an almost rectangular shape, which is typical of capacitive or electric double-layer capacitor electrode materials. However, the BAA electrolyte shows a slight faradaic contribution in both the anodic and cathodic regions around 1.03–1.07 V. Meanwhile, a pair of redox peaks (1.2/1.23 V) can be observed for IAA at different scan rates, presumably following from its reaction with iodine. The peak current (i) can be linearly related to the scan rate (v) using b-value analysis, as described by the following equation: $\log(i) = \log(a) + b\log(v)$. As shown in Fig. 6c and d, the b-values of the two peaks of BAA and IAA are 0.803/0.788 and 0.903/0.831, respectively, suggesting that the charge–discharge process is synergistically controlled by capacitive and diffusion behaviors.[60,61] The contribution ratios of the capacitive and diffusive behaviors were analyzed using Dunn's method (Fig. 6e–f). The slightly lower b-value and capacitive distribution for IAA indicate that the system exhibits slightly more diffusion-controlled behavior than that observed for BAA, attributable to the reaction of the iodide ions. This finding aligns with the higher specific capacity achieved by IAA as more active sites are utilized in diffusion. In contrast, no redox peak was observed for the base electrolyte, $ZnSO_4$, indicating that the charge storage mode is electrostatic adsorption and does not affect the capacity (Fig. S22). In the galvanostatic charge–discharge experiments at 2 A g^{-1} (Fig. 6g), BAA and IAA exhibit relatively higher capacity and cycling stability compared to those exhibited by the base electrolyte. In particular, the IAA electrolyte demonstrates an initial capacity of 280 mAh g^{-1} (calculated based on the weight of AC), which is approximately 4 times that of the base electrolyte cell, and retains 83% of its capacity after 1500 cycles. Moreover, the cell with IAA shows only a slight overpotential change and demonstrates significant cycling stability at a high current density (5 A g^{-1}) (Fig. S23). This suggests that the amount of charge passing through the cell can be significantly increased by creating a stable interfacial layer.

The feasibility of using electrolyte additives in grid-stabilized Zn metal batteries was further validated by examining their multirate performance. The cell containing IAA exhibits excellent capacity characteristics and stable cycling across all current densities (Fig. 6h). The excellent rate performance also indicates that sufficient electron transfer reactions and fast ion diffusion occur at both the cathode and anode. Since the system studied herein resembles an electrochemical capacitor owing to the nature of the AC cathode, self-discharge is considered as a significant issue, as ions are electrostatically adsorbed on the surface of the AC instead of being stored in the bulk.[62] After 10

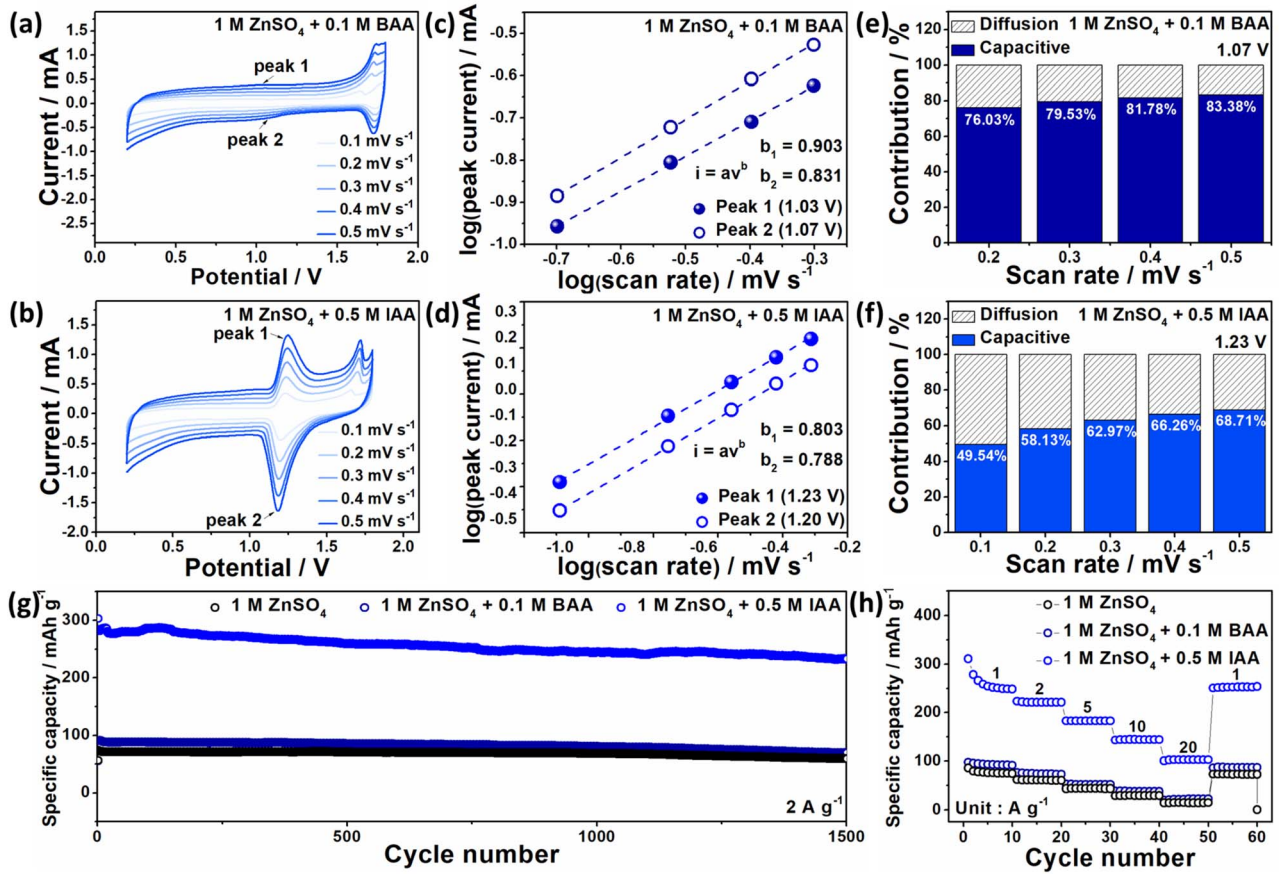

Fig. 6 Electrochemical performance of Zn||AC cells in 1 M $ZnSO_4$ electrolytes with and without haloacetamide additives. (a and b) Cyclic voltammetry curves at various scan rates for 1 M $ZnSO_4$ electrolytes containing (a) bromoacetamide and (b) iodoacetamide. (c and d) Log(-current)–log(scan rate) plots of peak current *versus* scan rate with linear fitting for (c) bromoacetamide and (d) iodoacetamide. (e and f) Capacitive contributions at different scan rates for (e) bromoacetamide and (f) iodoacetamide. (g) Galvanostatic charge–discharge curves at 2 A g^{-1} in 1 M $ZnSO_4$ electrolytes with and without bromoacetamide or iodoacetamide. (h) Multirate performance of Zn||AC cells in 1 M $ZnSO_4$ electrolytes with and without haloacetamide additives.

cycles of charge and discharge within a voltage range of 1.8–0.2 V at a current density of 2 A g^{-1}, the cells were allowed to rest for 24 h, and the actual energy loss was evaluated. As shown in Fig. S24, the cells with BAA and IAA achieve voltage retentions of 73% and 70%, respectively, after 24 h of rest. However, in the case of IAA, the capacity loss due to self-discharge is quickly recovered after additional cycling, demonstrating that the cell can rapidly restore stable performance even after self-discharge under practical conditions. This provides significant advantages in terms of long-term energy efficiency and stability. Overall, the results of the analyses indicate slight differences in the physicochemical and electrochemical performances of the selected BAA and IAA additives. Notably, as compared with bromide ions, iodide ions more effectively serve as anions for AZMBs. The interaction of iodoacetamide with Zn^{2+} ions and water molecules modifies the interface between the electrolyte and Zn anode, thereby ensuring uniform Zn plating/stripping and effectively suppressing dendrite formation. Consequently, the cell with the IAA-containing electrolyte exhibits reduced electrochemical overpotential and enhanced electrochemical stability.

4 Conclusions

The purpose of this study was to understand the effects of different halogen-containing acetamide derivatives as electrolyte additives for AZMBs. The addition of haloacetamides to a common base electrolyte, 1 M $ZnSO_4$, led to several interesting properties. First, according to DFT calculations, most haloacetamide derivatives effectively suppressed water decomposition and promoted the adsorption of ionized additive molecules onto the Zn surface. Second, not all the halide ions aided the formation of stable SEI layers on Zn. Third, the reactivity of haloacetamides drives the performance enhancement rather than the mere presence of halide anions. Finally, differences in the electrochemical performance were observed depending on the type and concentration of additives. In particular, iodoacetamide interacted with Zn^{2+} ions and water molecules to modify the interface between the electrolyte and Zn anode, ensuring uniform Zn plating and stripping, and suppressing dendrite formation. As a result, the iodoacetamide additive significantly reduced the electrochemical overpotential, thereby lowering polarization and enhancing electrochemical stability.

Among the halogens, iodine atoms can offer the best performance improvement as confirmed from the Zn symmetric cell cycling performance of haloacetamides and simple halide salts. We believe that a deeper understanding of the chemical interactions involved in the protection of Zn from halide anion-containing additives in electrolytes will be beneficial for the development of advanced electrolytes for AZMB applications.

Author contributions

Seul Gi Lee: conceptualization, formal analysis, investigation, writing – original draft. Syryll Olidan: data curation, formal analysis, software, investigation. Laudimer Tye Tan: software, visualization. Jihoon Kim: methodology, supervision. Kuk Young Cho: validation, supervision. Sukeun Yoon: conceptualization, supervision, funding acquisition, writing – review & editing.

Conflicts of interest

There are no conflicts to declare.

Data availability

The data supporting this article have been included as part of the supplementary information (SI). Supplementary information: calculation formulae for the Zn-ion transference number, COMSOL Multiphysics simulation procedure, chronopotentiometry profiles, cyclic voltammetry curves, EIS spectra, overpotential comparison, *in situ* optical microscopy images, pH measurements, X-ray diffraction patterns, SEM images, galvanostatic charge–discharge curves, and self-discharge behavior. See DOI: https://doi.org/10.1039/d5ta08741d.

Acknowledgements

This research was supported by grants from the Korea Institute for Advancement of Technology (KIAT) funded by the Ministry of Trade, Industry & Energy (MOTIE, Korea) (RS-2025-02310686 and P0017012), as well as by the Technology Innovation Program (RS-2024-00438338) through the Korea Planning & Evaluation Institute of Industrial Technology (KEIT), also funded by MOTIE.

Notes and references

1 S. Lou, F. Zhang, C. Fu, M. Chen, Y. Ma, G. Yin and J. Wang, Interface Issues and Challenges in All-Solid-State Batteries: Lithium, Sodium, and Beyond, *Adv. Mater.*, 2021, **33**, 2000721.
2 J.-M. Tarascon and M. Armand, Issues and Challenges Facing Rechargeable Lithium Batteries, *Nature*, 2001, **414**, 359–367.
3 J. B. Goodenough and Y. Kim, Challenges for Rechargeable Li Batteries, *Chem. Mater.*, 2010, **22**, 587–603.
4 Y. Liang, H. Dong, D. Aurbach and Y. Yao, Current Status and Future Directions of Multivalent Metal-Ion Batteries, *Nat. Energy*, 2020, **5**, 646–656.
5 T. Mageto, S. D. Bhoyate, K. Mensah-Darkwa, A. Kumar and R. K. Gupta, Development of High-Performance Zinc-Ion Batteries: Issues, Mitigation Strategies, and Perspectives, *J. Energy Storage*, 2023, **70**, 108081.
6 J. Ming, J. Guo, C. Xia, W. Wang and H. N. Alshareef, Zinc-Ion Batteries: Materials, Mechanisms, and Applications, *Mater. Sci. Eng. R Rep.*, 2019, **135**, 58–84.
7 Z. Liu, T. Cui, G. Pulletikurthi, A. Lahiri, T. Carstens, M. Olschewski and F. Endres, Dendrite-Free Nanocrystalline Zinc Electrodeposition from an Ionic Liquid Containing Nickel Triflate for Rechargeable Zn-Based Batteries, *Angew. Chem., Int. Ed.*, 2016, **55**, 2889–2893.
8 W. Lu, C. Xie, H. Zhang and X. Li, Inhibition of Zinc Dendrite Growth in Zinc-Based Batteries, *ChemSusChem*, 2018, **11**, 3996–4006.
9 K. Xie, K. Ren, C. Sun, S. Yang, M. Tong, S. Yang, Z. Liu and Q. Wang, Toward Stable Zinc-Ion Batteries: Use of a Chelate Electrolyte Additive for Uniform Zinc Deposition, *ACS Appl. Energy Mater.*, 2022, **5**, 4170–4178.
10 Z. Chen, Y. Tang, X. Du, B. Chen, G. Lu, X. Han, Y. Zhang, W. Yang, P. Han, J. Zhao and G. Cui, Anion Solvation Reconfiguration Enables High-Voltage Carbonate Electrolytes for Stable Zn/Graphite Cells, *Angew. Chem., Int. Ed.*, 2020, **59**, 21769–21777.
11 W. Xu, K. Zhao, W. Huo, Y. Wang, G. Yao, X. Gu, H. Cheng, L. Mai, C. Hu and X. Wang, Diethyl Ether as Self-Healing Electrolyte Additive Enabled Long-Life Rechargeable Aqueous Zinc Ion Batteries, *Nano Energy*, 2019, **62**, 275–281.
12 S. Wang, Y. Zhao, H. Lv, X. Hu, J. He, C. Zhi and H. Li, Low-Concentration Redox-Electrolytes for High-Rate and Long-Life Zinc Metal Batteries, *Small*, 2024, **20**, 2207664.
13 X. Huang, Q. Li, X. Zhang, H. Cao, J. Zhao, Y. Liu, Q. Zheng, Y. Huo, F. Xie, B. Xu and D. Lin, Critical Triple Roles of Sodium Iodide in Tailoring the Solventized Structure, Anode-Electrolyte Interface and Crystal Plane Growth to Achieve Highly Reversible Zinc Anodes for Aqueous Zinc-Ion Batteries, *J. Colloid Interface Sci.*, 2023, **650**, 875–882.
14 H. Yang, L. Li, D. Chen, J. Wang, Y. Tan, Z. Jiang, Y. Zhang, C. Miao, W. Zhang, W. Han and G. He, Stimulating the Potential of Zn Anodes to Operate in Low pH and Harsh Environments for Highly Sustainable Zn Batteries, *Angew. Chem., Int. Ed.*, 2025, **64**, e202419394.
15 J. Shin, J. Lee, Y. Park and J. W. Choi, Aqueous Zinc Ion Batteries: Focus on Zinc Metal Anodes, *Chem. Sci.*, 2020, **11**, 2028–2044.
16 T. Wang, C. Li, X. Xie, B. Lu, Z. He, S. Liang and J. Zhou, Anode Materials for Aqueous Zinc Ion Batteries: Mechanisms, Properties, and Perspectives, *ACS Nano*, 2020, **14**, 16321–16347.
17 P. Jaumaux, S. Wang, S. Zhao, B. Sun and G. Wang, Electrolyte Solvation Structure Design for High Voltage Zinc-Based Hybrid Batteries, *Energy Environ. Mater.*, 2023, **6**, e12578.

18 J. Yan, E. H. Ang, Y. Yang, Y. Zhang, M. Ye, W. Du and C. C. Li, High-Voltage Zinc-Ion Batteries: Design Strategies and Challenges, *Adv. Funct. Mater.*, 2021, **31**, 2010213.

19 M. Xi, Z. Liu, J. Ding, W. Cheng, D. Jia and H. Lin, Saccharin Anion Acts as a "Traffic Assistant" of Zn^{2+} to Achieve a Long-Life and Dendritic-Free Zinc Plate Anode, *ACS Appl. Mater. Interfaces*, 2021, **13**, 29631–29640.

20 X. Feng, P. Li, J. Yin, Z. Gan, Y. Gao, M. Li, Y. Cheng, X. Xu, Y. Su and S. Ding, Enabling Highly Reversible Zn Anode by Multifunctional Synergistic Effects of Hybrid Solute Additives, *ACS Energy Lett.*, 2023, **8**, 1192–1200.

21 S. Ilic, M. J. Counihan, S. N. Lavan, Y. Yang, Y. Jiang, D. Dhakal, J. Mars, E. N. Antonio, L. K. Iglesias, T. T. Fister, Y. Zhang, E. J. Maginn, M. F. Toney, R. F. Klie, J. G. Connell and S. Tepavcevic, Effect of Antisolvent Additives in Aqueous Zinc Sulfate Electrolytes for Zinc Metal Anodes: The Case of Acetonitrile, *ACS Energy Lett.*, 2024, **9**, 201–208.

22 T. N. T. Tran, M. Zhao, S. Geng and D. G. Ivey, Ethylene Glycol as an Antifreeze Additive and Corrosion Inhibitor for Aqueous Zinc-Ion Batteries, *Batter. Supercaps*, 2022, **5**, e202100420.

23 D. Wang, X. Guo, Z. Chen, Y. Zhao, Q. Li and C. Zhi, Ionic Liquid-Softened Polymer Electrolyte for Anti-Drying Flexible Zinc Ion Batteries, *ACS Appl. Mater. Interfaces*, 2022, **14**, 27287–27293.

24 L. Zhang, G. Wang, J. Feng, Q. Ma, Z. Liu and X. Yan, Designing a $Zn(BF_4)_2$-Based Ionic Liquid Electrolyte to Realize Superior Energy Density in a Carbon-Based Zinc-Ion Hybrid Capacitor, *Chemelectrochem*, 2021, **8**, 1289–1297.

25 J. Wan, R. Wang, Z. Liu, L. Zhang, F. Liang, T. Zhou, S. Zhang, L. Zhang, Q. Lu, C. Zhang and Z. Guo, A Double-Functional Additive Containing Nucleophilic Groups for High-Performance Zn-Ion Batteries, *ACS Nano*, 2023, **17**, 1610–1621.

26 Z. Huang, T. Wang, H. Song, X. Li, G. Liang, D. Wang, Q. Yang, Z. Chen, L. Ma, Z. Liu, B. Gao, J. Fan and C. Zhi, Effects of Anion Carriers on Capacitance and Self-Discharge Behaviors of Zinc Ion Capacitors, *Angew. Chem., Int. Ed.*, 2021, **60**, 1011–1021.

27 Z. Liu, G. Pulletikurthi, A. Lahiri, T. Cui and F. Endres, Suppressing the Dendritic Growth of Zinc in an Ionic Liquid Containing Cationic and Anionic Zinc Complexes for Battery Applications, *Dalton Trans.*, 2016, **45**, 8089–8098.

28 N. Zhang, F. Cheng, Y. Liu, Q. Zhao, K. Lei, C. Chen, X. Liu and J. Chen, Cation-Deficient Spinel $ZnMn_2O_4$ Cathode in $Zn(CF_3SO_3)_2$ Electrolyte for Rechargeable Aqueous Zn-Ion Battery, *J. Am. Chem. Soc.*, 2016, **138**, 12894–12901.

29 L. Cao, D. Li, E. Hu, J. Xu, T. Deng, L. Ma, Y. Wang, X.-Q. Yang and C. Wang, Solvation Structure Design for Aqueous Zn Metal Batteries, *J. Am. Chem. Soc.*, 2020, **142**, 21404–21409.

30 C. Xie, H. Zhang, W. Xu, W. Wang and X. Li, A Long Cycle Life, Self-Healing Zinc–Iodine Flow Battery with High Power Density, *Angew. Chem., Int. Ed.*, 2018, **57**, 11171–11176.

31 Y. Hiranuma, K. Kaniwa, M. Shoji and F. Mafuné, Solvation Structures of Iodide on and below a Surface of Aqueous Solution Studied by Photodetachment Spectroscopy, *J. Phys. Chem. A*, 2011, **115**, 8493–8497.

32 L. Falciola, P. R. Mussini, S. Trasatti and L. M. Doubova, Specific Adsorption of Bromide and Iodide Anions from Nonaqueous Solutions on Controlled-Surface Polycrystalline Silver Electrodes, *J. Electroanal. Chem.*, 2006, **593**, 185–193.

33 F. Xie, H. Li, X. Wang, X. Zhi, D. Chao, K. Davey and S.-Z. Qiao, Mechanism for Zincophilic Sites on Zinc-Metal Anode Hosts in Aqueous Batteries, *Adv. Energy Mater.*, 2021, **11**, 2003419.

34 Q. Guan, J. Li, L. Li, P. Chai, Y. Li, S. Zhang, X. Yu, L. Bao, J. Peng and X. Li, In Situ Construction of Organic Anion-Enriched Interface Achieves Ultra-Long Life Aqueous Zinc-Ion Battery, *Chem. Eng. J.*, 2023, **476**, 146534.

35 V. Yrjänä, DearEIS - A GUI Program for Analyzing Impedance Spectra, *J. Open Source Softw.*, 2022, **7**, 4808.

36 P. Giannozzi, S. Baroni, N. Bonini, M. Calandra, R. Car, C. Cavazzoni, D. Ceresoli, G. L. Chiarotti, M. Cococcioni, I. Dabo, A. Dal Corso, S. de Gironcoli, S. Fabris, G. Fratesi, R. Gebauer, U. Gerstmann, C. Gougoussis, A. Kokalj, M. Lazzeri, L. Martin-Samos, N. Marzari, F. Mauri, R. Mazzarello, S. Paolini, A. Pasquarello, L. Paulatto, C. Sbraccia, S. Scandolo, G. Sclauzero, A. P. Seitsonen, A. Smogunov, P. Umari and R. M. Wentzcovitch, QUANTUM ESPRESSO: A Modular and Open-Source Software Project for Quantum Simulations of Materials, *J. Phys.: Condens. Matter*, 2009, **21**, 395502.

37 C. Ma, K. Yang, S. Zhao, Y. Xie, C. Liu, N. Chen, C. Wang, D. Wang, D. Zhang, Z. X. Shen and F. Du, Recyclable and Ultrafast Fabrication of Zinc Oxide Interface Layer Enabling Highly Reversible Dendrite-Free Zn Anode, *ACS Energy Lett.*, 2023, **8**, 1201–1208.

38 D. Wang, D. Lv, H. Liu, S. Zhang, C. Wang, C. Wang, J. Yang and Y. Qian, In Situ Formation of Nitrogen-Rich Solid Electrolyte Interphase and Simultaneous Regulating Solvation Structures for Advanced Zn Metal Batteries, *Angew. Chem., Int. Ed.*, 2022, **61**, e202212839.

39 Y. Chen, F. Gong, W. Deng, H. Zhang and X. Wang, Dual-Function Electrolyte Additive Enabling Simultaneous Electrode Interface and Coordination Environment Regulation for Zinc-Ion Batteries, *Energy Stor. Mater.*, 2023, **58**, 20–29.

40 M. Qiu, L. Ma, P. Sun, Z. Wang, G. Cui and W. Mai, Manipulating Interfacial Stability Via Absorption-Competition Mechanism for Long-Lifespan Zn Anode, *Nano-Micro Lett.*, 2021, **14**, 31.

41 I. B. Obot, S. A. Umoren and N. O. Obi-Egbedi, Corrosion Inhibition and Adsorption Behaviour for Aluminuim by Extract of Aningeria Robusta in HCl Solution: Synergistic Effect of Iodide Ions, *J. Mater. Environ. Sci.*, 2011, **2**, 60–71.

42 M. E. King and M. L. Personick, Iodide-Induced Differential Control of Metal Ion Reduction Rates: Synthesis of Terraced Palladium–Copper Nanoparticles with Dilute Bimetallic Surfaces, *J. Mater. Chem. A*, 2018, **6**, 22179–22188.

43 J.-H. Cho and Y.-H. Kim, Reduction of 2,4,6-Trichlorophenol with Zero-Valent Zinc and Catalyzed Zinc, *J. Hazard. Mater.*, 2009, **166**, 984–991.

44 C. Ratanaphain, D. Viboonratanasri, P. Prompinit, S. Krajangpan, E. Khan and P. Punyapalakul, Reactivity Characterization of SiO_2-Coated Nano Zero-Valent Iron for Iodoacetamide Degradation: The Effects of SiO_2 Thickness, and the Roles of Dehalogenation, Hydrolysis and Adsorption, *Chemosphere*, 2022, **286**, 131816.

45 C. Ratanaphain, D. Viboonratanasri, P. Prompinit, S. Krajangpan, E. Khan and P. Punyapalakul, Mechanistic Study of Iodoacetamide Degradation by Functionalized SiO2-Coated nZVI: The Role of Surface Functional Groups on Adsorption, Dehalogenation and Hydrolysis, *J. Water Process Eng.*, 2024, **63**, 105485.

46 L.-Y. Lin and C.-C. Chen, Accurate Characterization of Transference Numbers in Electrolyte Systems, *J. Power Sources*, 2024, **603**, 234236.

47 A. J. Bard, *Integrated Chemical Systems: A Chemical Approach to Nanotechnology*, Wiley, New York, 1994.

48 Z. Liu, R. Wang, Y. Gao, S. Zhang, J. Wan, J. Mao, L. Zhang, H. Li, J. Hao, G. Li, L. Zhang and C. Zhang, Low-Cost Multi-Function Electrolyte Additive Enabling Highly Stable Interfacial Chemical Environment for Highly Reversible Aqueous Zinc Ion Batteries, *Adv. Funct. Mater.*, 2023, **33**, 2308463.

49 S.-J. Zhang, J. Hao, D. Luo, P.-F. Zhang, B. Zhang, K. Davey, Z. Lin and S.-Z. Qiao, Dual-Function Electrolyte Additive for Highly Reversible Zn Anode, *Adv. Funct. Mater.*, 2021, **11**, 2102010.

50 J. Li, S. Zhang, X. Yu, J. Li, H. Gu, Y. Long, N. Li, J. Han and Z. Yang, Enhancing Long-Term Cycling Stability in Aqueous Zinc-Ion Batteries via Effective Control of Bulk Electrolyte with Biomass-Derived Multifunctional Additive, *Nano Energy*, 2025, **141**, 111049.

51 Y. Quan, M. Yang, M. Chen, W. Zhou, X. Han, J. Chen, B. Liu, S. Shi and P. Zhang, Electrolyte Additive of Sorbitol Rendering Aqueous Zinc-Ion Batteries with Dendrite-Free Behavior and Good Anti-Freezing Ability, *Chem. Eng. J.*, 2023, **458**, 141392.

52 M. Yan, C. Xu, Y. Sun, H. Pan and H. Li, Manipulating Zn Anode Reactions through Salt Anion Involving Hydrogen Bonding Network in Aqueous Electrolytes with PEO Additive, *Nano Energy*, 2021, **82**, 105739.

53 S. Zhang, M. Ye, Y. Zhang, Y. Tang, X. Liu and C. C. Li, Regulation of Ionic Distribution and Desolvation Activation Energy Enabled by In Situ Zinc Phosphate Protective Layer toward Highly Reversible Zinc Metal Anodes, *Adv. Funct. Mater.*, 2023, **33**, 2208230.

54 F. Mo, Z. Chen, G. Liang, D. Wang, Y. Zhao, H. Li, B. Dong and C. Zhi, Zwitterionic Sulfobetaine Hydrogel Electrolyte Building Separated Positive/Negative Ion Migration Channels for Aqueous Zn-MnO_2 Batteries with Superior Rate Capabilities, *Adv. Energy Mater.*, 2020, **10**, 2000035.

55 B. W. Olbasa, F. W. Fenta, S.-F. Chiu, M.-C. Tsai, C.-J. Huang, B. A. Jote, T. T. Beyene, Y.-F. Liao, C.-H. Wang, W.-N. Su, H. Dai and B. J. Hwang, High-Rate and Long-Cycle Stability with a Dendrite-Free Zinc Anode in an Aqueous Zn-Ion Battery Using Concentrated Electrolytes, *ACS Appl. Energy Mater.*, 2020, **3**, 4499–4508.

56 Q. Meng, R. Zhao, P. Cao, Q. Bai, J. Tang, G. Liu, X. Zhou and J. Yang, Stabilization of Zn Anode via a Multifunctional Cysteine Additive, *Chem. Eng. J.*, 2022, **447**, 137471.

57 W. Zhang, Y. Dai, R. Chen, Z. Xu, J. Li, W. Zong, H. Li, Z. Li, Z. Zhang, J. Zhu, F. Guo, X. Gao, Z. Du, J. Chen, T. Wang, G. He and I. P. Parkin, Highly Reversible Zinc Metal Anode in a Dilute Aqueous Electrolyte Enabled by a pH Buffer Additive, *Angew. Chem., Int. Ed.*, 2023, **62**, e202212695.

58 Z. Xiang, Y. Qiu, X. Guo, K. Qi, Z.-L. Xu and B. Y. Xi, Inherited Construction of Porous Zinc Hydroxide Sulfate Layer for Stable Dendrite-Free Zn Anode, *Energy Environ. Sci.*, 2024, **17**, 3409–3418.

59 K. Huang, X. Zeng, D. Zhang, C. Wen, C. Lu, W. Wu, Y. Guo and J. Xing, Regulation of Zinc Hydroxide Sulfate Growth Environment for Stable Zinc Anode/Electrolyte Interfaces, *Langmuir*, 2025, **41**, 2735–2743.

60 J. Liu, J. Wang, C. Xu, H. Jiang, C. Li, L. Zhang, J. Lin and Z. X. Shen, Advanced Energy Storage Devices: Basic Principles, Analytical Methods, and Rational Materials Design, *Adv. Sci.*, 2018, **5**, 1700322.

61 Y. Jiang and J. Liu, Definitions of Pseudocapacitive Materials: A Brief Review, *Energy Environ. Mater.*, 2019, **2**, 30–37.

62 J. Yang, M. A. Bissett and R. A. W. Dryfe, Investigation of Voltage Range and Self-Discharge in Aqueous Zinc-Ion Hybrid Supercapacitors, *ChemSusChem*, 2021, **14**, 1700–1709.

